
EverybodyDance: Bipartite Graph–Based Identity Correspondence for Multi-Character Animation

Haotian Ling^{1,2*} Zequn Chen^{2†} Qiuying Chen³
 Donglin Di² Yongjia Ma² Hao Li² Chen Wei² Zhulin Tao^{3‡} Xun Yang^{1,4‡}

¹University of Science and Technology of China ²Li Auto ³Communication University of China

⁴MoE Key Laboratory of Brain-inspired Intelligent Perception and Cognition, USTC

haotianling@mail.ustc.edu.cn, xyang21@ustc.edu.cn
 {chenzequn, didonglin, mayongjia, lihao43, chenwei10}@lixiang.com
 chenqy@cuc.edu.cn, taozl@cuc.edu.cn

Abstract

Consistent pose-driven character animation has achieved remarkable progress in single-character scenarios. However, extending these advances to multi-character settings is non-trivial, especially when position swap is involved. Beyond mere scaling, the core challenge lies in enforcing correct Identity Correspondence (IC) between characters in reference and generated frames. To address this, we introduce EverybodyDance, a systematic solution targeting IC correctness in multi-character animation. EverybodyDance is built around the **Identity Matching Graph (IMG)**, which models characters in the generated and reference frames as two node sets in a weighted complete bipartite graph. Edge weights, computed via our proposed Mask–Query Attention (MQA), quantify the affinity between each pair of characters. Our key insight is to formalize IC correctness as a graph structural metric and to optimize it during training. We also propose a series of targeted strategies tailored for multi-character animation, including identity-embedded guidance, a multi-scale matching strategy, and pre-classified sampling, which work synergistically. Finally, to evaluate IC performance, we curate the **Identity Correspondence Evaluation** benchmark, dedicated to multi-character IC correctness. Extensive experiments demonstrate that EverybodyDance substantially outperforms state-of-the-art baselines in both IC and visual fidelity.

1 Introduction

Character animation aims to generate video sequences from still images guided by specific pose sequences [1; 2]. Unlike text-driven generation focusing mainly on high-level semantic alignment [3; 4], it requires a dual fidelity: maintaining consistent visual appearance—including fine-grained details and accurately performing complex motion sequences [5; 6]. This requirement has generated significant research interest [7; 8; 9; 10; 11; 12].

Despite significant advances in single character animation generation (e.g. [8; 9; 13; 14; 12]), extending these methods to multi-character scenarios introduces unique challenges (see Figure 1). The key challenges are twofold. First, in multi-character scenarios, characters can swap relative

*Work done during an internship at Li Auto.

†Project Leader.

‡Corresponding authors.

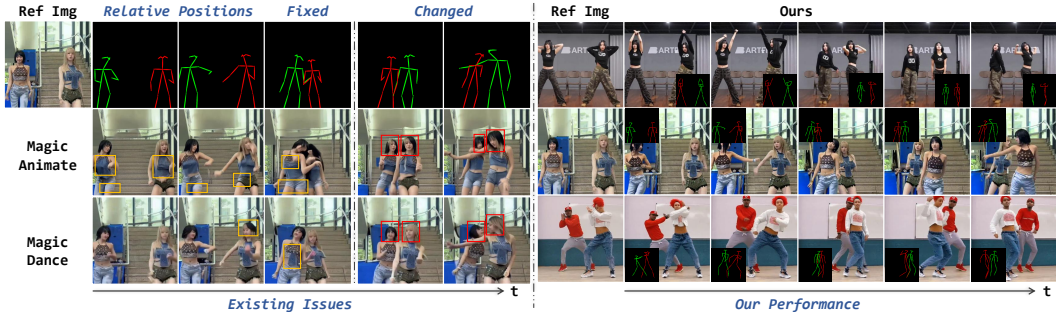


Figure 1: The left panel highlights the challenges of extending existing methods to multi-character scenarios. The yellow box indicates feature interference between characters, while the red box marks identity mismatches. The right panel illustrates our method’s accurate identity correspondence.

positions, leading to identity confusion. Furthermore, the appearances of different characters can interfere with one another. Existing single-character animation approaches [14; 13; 9; 10; 12] are mainly based on implicit data-driven paradigms. In multi-character scenarios, such paradigm struggles to guarantee accurate one-to-one correspondence between generated and reference characters (see Section 4.3). Empirical results demonstrate that state-of-the-art methods often struggle to achieve satisfactory Identity Correspondence (IC) under these conditions (see Section 4.2).

To address these limitations, we propose an explicit modeling framework, which directly captures the correspondence between generated characters and their reference counterparts. Our method enforces correct IC between characters during training. Specifically, we introduce a weighted complete bipartite graph, **Identity Matching Graph (IMG)**, whose two node sets represent generated/reference characters. Edge weights, derived by our proposed **Mask-Query Attention (MQA)**, quantify the affinity between each generated/reference pair. A global matching score derived from the IMG provides a direct, optimizable objective for IC correctness. Integrating IMG into training achieves disentanglement of multiple characters and yields more accurate IC for multi-character animations. The construction process of IMG is **dynamic**, making it scalable for any number of characters.

To resolve the ambiguity of motion guidance in multi-character scenarios, we designed **Identity Embedded Guidance (IEG)**. IEG provides clear anchors for each character throughout both training and inference. During the training phase, IEG and IMG work synergistically to create a guidance-supervision loop. To further strengthen the robustness of IC, we employ a suite of targeted improvements. First, to enforce the correct correspondence across the entire feature hierarchy, we introduce a multi-scale matching strategy. In addition, to address the long-tail distribution of the multi-character dataset, we propose a pre-classified sampling strategy to ensure that difficult and infrequent position-swap samples receive sufficient emphasis during training. To rigorously evaluate IC performance under complex multi-character conditions, we also present the Identity Correspondence Evaluation (ICE) benchmark, designed to challenge and compare SOTA methods on their ability to maintain correct IC.

Our main contributions are summarized as follows: **(1) Graph-Based IC Modeling:** We propose the Identity Matching Graph (IMG), a weighted complete bipartite graph that explicitly models IC in multi-character animation, whose edge weights are computed via our proposed Mask-Query Attention (MQA). **(2) Targeted Strategies:** We propose a series of targeted strategies, including identity-embedded pose guidance, a multi-scale matching strategy and a pre-classified sampling strategy, all tailored to multi-character animation. **(3) ICE Benchmark:** We curate the benchmark, ICE, for comprehensive evaluation in multi-character animation. Extensive evaluations demonstrate that our approach significantly outperforms SOTA baselines in both IC accuracy and visual fidelity.

2 Related Work

2.1 Diffusion Models

Diffusion Models gradually corrupt data by adding Gaussian noise and learn a reverse denoising process to model complex distributions [15; 16; 17; 18]. At inference, samples are generated by

starting from pure noise and iteratively denoising with the trained model [19; 20]. Extensions to latent diffusion operate in compressed feature spaces for efficient high-resolution and text-to-image generation [21]. Beyond images, diffusion frameworks produce temporally coherent videos for facial expression and dance generation [22; 9; 11]. Conditional diffusion enables flexible generation by guiding the reverse process with model-free or classifier-free cues [20; 23].

2.2 Video Generation

Early video synthesis relied on GAN-based [24] frameworks (e.g., TGAN [25]), which introduced temporal shift modules to enforce frame-to-frame coherence. Diffusion-based approaches [26] extend image diffusion models by integrating spatio-temporal conditioning or specialized temporal attention layers, as seen in Tune-A-Video’s [27] tailored spatio-temporal attention and MagicVideo’s [28] directed temporal attention module in latent space. Transformer-centric models such as Video Diffusion Transformer (VDT) [29] and Matten [30] leverage modular temporal and spatial attention (e.g., Mamba-Attention [31]) to capture long-range dependencies and global video context. Training-free extensions such as FreeLong [32] employ a SpectralBlend temporal attention mechanism to adapt pretrained short-clip diffusion models for long-video generation, maintaining both global consistency and local detail without additional training. Recent video super-resolution and editing techniques employ temporal-consistent diffusion priors to reduce flicker and preserve object appearance, further enhancing smoothness in tasks from animation to real-world scene synthesis [33].

2.3 Human Image Animation

Early GAN-based methods [34; 6; 35; 36; 37; 38; 39; 40] used appearance flow for feature warping but suffered from adversarial training issues such as mode collapse and motion inaccuracy [9]. More recent work [12; 9; 10; 7; 8; 11; 13; 41; 42; 43; 44; 45; 46] based on diffusion models, which offers stable training [47]. Disco [8] uses ControlNet [48] for disentangled pose–foreground–background control. ReferenceNet [9] improves fine-detailed consistency by injecting the appearance of a reference frame into the denoising UNet. Recent work has also made valuable contributions to multi-character scenarios. Ingredients [49] focuses on text-controlled multi-character layout, Follow-Your-Pose-V2 [50] focuses on scenes where characters maintain fixed relative positions.

3 Method

Identity Correspondence (IC), a one-to-one matching between each generated character and its counterpart in the reference frame, becomes especially critical when characters swap positions. Existing character animation methods [8; 9; 11; 13] typically rely on end-to-end training losses that capture only global similarity, often failing to enforce correct IC in such scenarios (see Section 4.3).

Section 3.1 introduces our formulation of the Identity Matching Graph (IMG). Section 3.2 explains how the IMG is constructed. Section 3.3 presents our targeted strategies for multi-character animation.

3.1 Problem Formulation

Concretely, we construct a weighted complete bipartite graph between the reference (ref) and the generated (gen) characters in each frame. The node set $\mathcal{R} = \{r_1, \dots, r_m\}$ represents m characters ordered from left to right in the reference frame (numbered 1 to m), while the node set $\mathcal{G} = \{g_1, \dots, g_n\}$ with $n \leq m$ describes n characters in the generated frame. We define the **Identity Matching Graph** (IMG) as the following bipartite graph:

$$\mathcal{B}_{\text{ID}} = (\mathcal{R}, \mathcal{G}, E, w), \quad E = \{(r_i, g_j) \mid 1 \leq i \leq m, 1 \leq j \leq n\}, \quad (1)$$

where the edge weight $w(r_i, g_j) \geq 0$ represents the affinity (potential correspondence) between r_i and g_j (see left panel of the Figure 2). **During training**, for each generated frame we construct its IMG, yielding the set \hat{E} of $n \times m$ edges (i.e., all possible correspondences between characters). We denote the edge set of n ground-truth correspondences by \mathcal{M}^* . Since the edges in \mathcal{M}^* represent the correct IC, our objective is to increase their weights by training the UNet [51]. Therefore, we use the following ratio \mathcal{C} to quantify the correctness of IC as:

$$\mathcal{C} = \frac{\sum_{(r_i, g_j) \in \mathcal{M}^*} w(r_i, g_j)}{\sum_{(r_i, g_j) \in \hat{E}} w(r_i, g_j)} \in [0, 1], \mathcal{M}^* \subseteq \hat{E}. \quad (2)$$

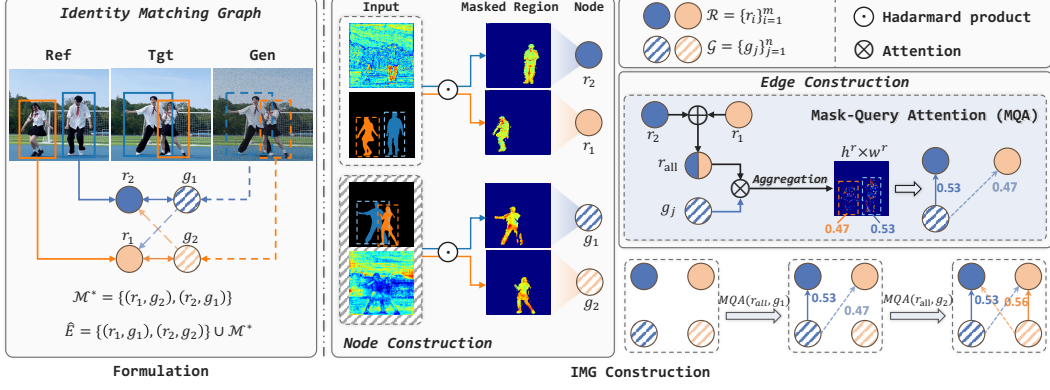


Figure 2: The left panel illustrates *what* is the IMG. The target (tgt) frame indicates the ground truth correspondence, indicating which edges belong to the set \mathcal{M}^* . The right panel shows *how* we build the IMG. Since the regions in \mathcal{R} do not overlap spatially, we sum all $\{r_i\}_{i=1}^m$ representations into r_{all} .

Lower \mathcal{C} indicates a more severe ambiguity. Optimizing \mathcal{C} will force the model to learn correct IC, which will serve as a loss term during the training of the diffusion model. **For example**, in the left panel of Figure 2, if the left generated character g_1 has a higher affinity to reference character r_1 than its true counterpart r_2 , by the IMG construction in Section 3.2, the edge weight for (r_2, g_1) will be a low value. Under the total loss defined in Equation 8, this low-weighted pairing incurs a penalty, thereby driving the model to learn the correct inter-character correspondence.

3.2 Identity Matching Graph Construction

Node Construction. During training, the reference and generated frames are encoded into the latent space [47]. Therefore, we propose to use the corresponding masked regions in the latent space to represent each character, and then build the IMG nodes from those regions. We denote $\{M_i^r\}_{i=1}^m$ as the instance segmentation [52] masks of the m reference characters, and $\{M_j^g\}_{j=1}^n$ represents the masks of the n ($n \leq m$) generated characters. Since instance segmentation is performed offline on the training set, we extract the masks for the generated frames from their corresponding ground-truth target frames. This approach circumvents potential drawbacks in both efficiency and accuracy.

In a chosen UNet [51] layer ℓ , we extract the intermediate reference and generated feature, denoted as $\mathbf{f}^r \in \mathbb{R}^{c \times h^r \times w^r}$, $\mathbf{f}^g \in \mathbb{R}^{c \times h^g \times w^g}$, respectively. (h^r, w^r) and (h^g, w^g) are the sizes of the reference and generated latent maps. Each mask is interpolated to match the spatial resolution of the corresponding latent feature map: $\widetilde{M}_i^r = \text{Interp}(M_i^r) \in \{0, 1\}^{h^r \times w^r}$, $\widetilde{M}_j^g = \text{Interp}(M_j^g) \in \{0, 1\}^{h^g \times w^g}$. The latent regions corresponding to these segmentation masks are treated as graph nodes r_i, g_j as:

$$r_i = \mathbf{f}^r \odot \widetilde{M}_i^r, \quad g_j = \mathbf{f}^g \odot \widetilde{M}_j^g, \quad (3)$$

\odot denotes the Hadamard product, yielding reference nodes $\{r_i\}_{i=1}^m$ and generated nodes $\{g_j\}_{j=1}^n$.

Edge Construction. To compute the edge weight $w(r_i, g_j)$ of the IMG, we propose the **Mask-Query Attention** to estimate the affinity between g_j and r_i . It exploits the ability of the attention mechanism's [53; 9] to capture spatial dependence. Each generated character $\{g_j\}_{j=1}^n$ is transformed into a query matrix $Q_j \in \mathbb{R}^{(h^g \cdot w^g) \times d}$, and transfer each reference character $\{r_i\}_{i=1}^m$ to a key $K_i \in \mathbb{R}^{(h^r \cdot w^r) \times d}$. The attention map A_i^j between r_i and g_j is calculated as:

$$A_i^j = \text{softmax}\left(\frac{Q_j K_i^\top}{\sqrt{d}}\right) \in \mathbb{R}^{(h^g \cdot w^g) \times (h^r \cdot w^r)}. \quad (4)$$

$A_i^j[p, q]$ denotes the dependence from the p -th patch of g_j to the q -th patch of r_i . We use the score S_i^j to reflect the affinity between generated character g_j and reference character r_i :

$$S_i^j = \sum_{q \in \mathcal{V}_i^r} \sum_{p \in \mathcal{V}_j^g} A_i^j[p, q], \quad \mathcal{V}_j^g = \{p \mid \widetilde{M}_j^g[p] = 1\}, \quad \mathcal{V}_i^r = \{q \mid \widetilde{M}_i^r[q] = 1\} \quad (5)$$

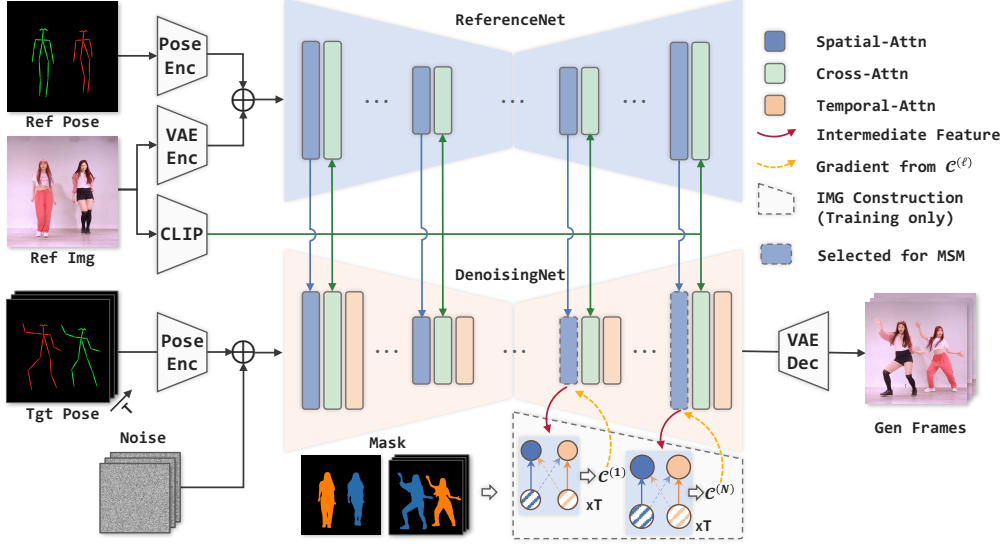


Figure 3: Training pipeline of EverybodyDance. We only construct the IMG during training. We additionally input the IEG of the reference image. ReferenceNet binds character identity by fusing the reference image’s appearance to create identity-aware features that guide the DenoisingNet.

Equation 5 aggregates patch-level dependency A_i^j into a node-level affinity score S_i^j , which reflects the overall correlation between the generated character g_j and the reference character r_i . In the attention map A_i^j , each row corresponds to a patch in the generated latent g_j , and each column corresponds to a patch in the reference latent r_i . To quantify the relative affinity between g_j and each reference character $\{r_i\}_{i=1}^m$, we first compute the set of affinity scores $\{S_i^j\}_{i=1}^m$. Each score S_i^j aggregates patch-level attention scores from A_i^j across the masked regions defined by \widetilde{M}_j^g and \widetilde{M}_i^r . We then normalize these scores to obtain the final edge weights $\{w(r_i, g_j)\}_{i=1}^m$:

$$w(r_i, g_j) = \frac{S_i^j}{\sum_{i=1}^m S_i^j + \gamma} \in [0, 1), \quad \gamma = 10^{-8}. \quad (6)$$

Computing the pair-wise attention A_i^j for all $m \times n$ pairs is inefficient. As shown in Figure 2, we aggregate all reference nodes into a single representation, $r_{all} = \sum_{i=1}^m r_i$. Each generated node g_j then computes attention against r_{all} . This optimization reduces the computational complexity from $\mathcal{O}(m \cdot n)$ to $\mathcal{O}(n)$. Since m and n are dynamically determined by the number of segmentation masks, the IMG is built in a fully **dynamic** process that can be extended to any number of characters.

3.3 Targeted Strategies

Identity-Embedded Guidance Existing methods rely solely on pose guidance without incorporating explicit identity information [54; 55; 35; 56], which complicates multi-character animation by lacking reliable identity cues for correct Identity Correspondence (IC). To resolve this, we introduce Identity-Embedded Guidance (IEG), which embeds identity into DWPose [54] by color-coding each skeleton (see Appendix for details). The IEG from each reference frame is also injected into its feature space.

These colored skeletons serve to mark reference characters and guide the placement of corresponding characters during generation, thereby enabling the model to differentiate identities during training and inference. We provide explicit input cues (IEG) and a matching loss (IMG). Both originate from the same segmentation masks to ensure alignment between guidance and supervision.

Multi-Scale Matching To improve training robustness and ensure correct IC across different feature spaces, we perform Multi-Scale Matching (MSM) at N selected UNet [51] layers $\{\ell\}_{\ell=1}^N$. At each

Table 1: Quantitative comparison on the ICE benchmark. Arrows indicate optimal direction (\downarrow =lower better, \uparrow =higher better). AnimateAnyone* denotes the model fine-tuned on our dataset.

Method	Frame Quality				Video Quality		
	SSIM \uparrow	PSNR* \uparrow	LPIPS \downarrow	L1 \downarrow	FID \downarrow	FID-VID \downarrow	FVD \downarrow
AnimateAnyone [9]	0.616	14.97	0.339	5.16E-05	59.19	32.057	364.85
AnimateAnyone* [9]	0.596	14.67	0.342	5.35E-05	54.71	31.274	358.31
MimicMotion [14]	0.621	15.00	0.338	5.48E-05	60.77	26.490	381.69
MagicDance [12]	0.508	13.81	0.424	1.33E-04	53.30	47.127	471.71
MagicAnimate [10]	0.614	13.95	0.369	6.36E-05	76.28	42.257	521.67
UniAnimate [13]	0.623	15.66	0.328	3.41E-05	44.38	26.696	295.56
EverybodyDance	0.654	16.93	0.304	2.86E-05	40.19	23.584	225.06

layer ℓ we construct its IMG $B_{\text{ID}}^{(\ell)}$ and compute layer-level IC score according to Equation 2:

$$c^{(\ell)} = \frac{\sum_{(r_i, g_j) \in \mathcal{M}^*} w^{(\ell)}(r_i, g_j)}{\sum_{(r_i, g_j) \in \hat{\mathcal{E}}^{(\ell)}} w^{(\ell)}(r_i, g_j)} \in [0, 1], \quad (7)$$

where $w^{(\ell)}(r_i, g_j)$ are the edge weights at layer ℓ , \mathcal{M}^* are the ground-truth correspondences, and $\hat{\mathcal{E}}^{(\ell)}$ is the full bipartite edge set at that layer. We then use the average of $\{-\mathcal{C}^\ell\}^{1:N}$ over all N layers to be the matching loss $\mathcal{L}_{\text{match}}$. Minimizing $\mathcal{L}_{\text{match}}$ thus encourages the model to maximize IC correctness across all chosen scales, yielding more robust multi-character generation with accurate IC. The full pipeline is illustrated in Figure 3. The final training objective consists of standard diffusion reconstruction loss $\mathcal{L}_{\text{diff}}$ and $\mathcal{L}_{\text{match}}$, denoted as:

$$\mathcal{L} = \mathcal{L}_{\text{diff}} + \lambda \mathcal{L}_{\text{match}}, \quad \lambda > 0, \quad (8)$$

where λ balances the frame quality against IC correctness.

Pre-Classified Sampling Existing methods [11; 9; 10] typically select reference–target frame pairs randomly from a training video. However, in multi-character scenarios, challenging sample pairs, such as those involving position swaps, are relatively rare. To address this, we extract the position of each character. Then, with probability ρ we draw from the pre-classified challenging swap pairs, and with probability $1 - \rho$ we conduct random sampling.

4 Experiment

4.1 Settings

Quantitative Metrics. To quantitatively evaluate the performance of different methods, we employ several widely used metrics, including L1 [57], PSNR* [58; 6], SSIM [59], LPIPS [60], FID [24], FID-VID [24], and FVD [61]. These metrics jointly provide a comprehensive evaluation.

Baselines. To validate the superiority of our method, we conduct extensive comparisons against several SOTA methods: MagicAnimate [10], AnimateAnyone [9], MagicPose [12], MimicMotion [14], Follow-Your-Pose-V2 [50] and UniAnimate [13].

Dataset and Other Details. We curated a custom multi-character dataset comprising approximately 800 video clips. For IC correctness evaluation, we introduce the ICE-bench, which contains 3,200 video frames. Our model is fine-tuned based on the AnimateAnyone framework using this dataset. For full descriptions of the training dataset and ICE-bench, other experiments, please refer to the Appendix.

4.2 Comparison Study

We evaluate our method, **EverybodyDance**, on the ICE-Bench using both quantitative metrics and qualitative showcases. As reported in Table 1, EverybodyDance achieves substantial improvements over its backbone model, AnimateAnyone: it reduces the FVD score by **38.3%**, indicating significantly improved video fidelity. To ensure these gains stem from our proposed targeted enhancements

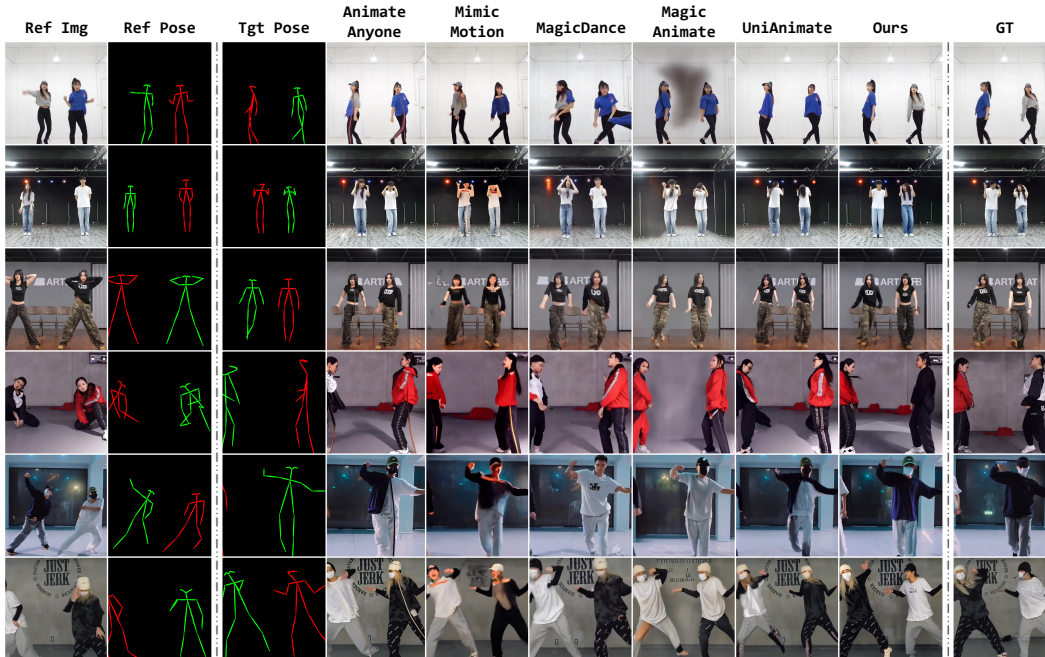


Figure 4: We compare our method with several state-of-the-art baselines. The last three rows illustrate three particularly challenging scenarios: (1) reference images exhibiting complex, non-standard poses; (2) target poses involving fewer character than the corresponding reference images; and (3) reference characters undergoing severe occlusion. Under these difficult conditions, our method consistently outperforms existing approaches, demonstrating accurate IC.

rather than dataset-specific biases, we additionally fine-tuned AnimateAnyone on our dataset; even so, it still fails to match the performance of EverybodyDance. Qualitatively, as shown in Figure 4 our approach consistently achieves accurate character identity correspondences in challenging scenarios such as position swaps, where existing methods often produce identity confusion or mismatches.

4.3 Ablation Study

To elucidate how our method enforces correct IC, we conduct a series of ablation experiments, summarized in Table 2. The experiments are categorized into the following three groups:

Effectiveness of the Identity Matching Graph We compare our IMG-based approach against several ablation variants: **1) t/w IEG**: We fine-tune the backbone model using IEG rather than DWPose. **2) End2End**: We provide the IEG of reference image, allowing the model to learn IC in an end-to-end scheme. **3) End2End-M**: We further use masks over each character’s region to enforce the model to focus on the corresponding region (see details in the Appendix).

As shown in the first group, introducing IEG alone yields some gains, while embedding identity cues (End2End and End2End-M) into the reference image’s feature space enables partial performance improvements but remains insufficient. Only when IMG is incorporated to explicitly supervise character-to-character correspondence, the model achieves a dramatic improvement.

We also present qualitative comparison results in Figure 5. Figure 6 visualizes attention maps for both the IMG-based and end-to-end paradigms. We present visualizations of r_{all} alongside each generated character g_j in Section 3.2. For each g_1 and g_2 , arranged from left to right, we display its affinity scores with all reference characters. To enable direct comparison, we include the corresponding attention map visualizations from the End2End-M model. In the table, the columns labeled $\text{IMG-}g_j$ and $\text{End2End-M-}g_j$ respectively illustrate the attention maps of g_1 and g_2 over the reference image.

Effectiveness of Multi-Scale Matching As demonstrated in the second group of experiments, a progressive increase in the number of matching layers leads to consistent improvements in overall performance.

Table 2: To facilitate analysis, the table is divided into three groups. MSM- N refers to building the IMG using the last N layers of the UNet, while PCS- ρ denotes selecting pre-classified hard samples with a sampling ratio of ρ . In the *Full* setting, we set $N = 5$ and $\rho = 0.3$.

Experiment Group	Experiment Settings	Frame Quality					Video Quality	
		SSIM \uparrow	PSNR* \uparrow	LPIPS \downarrow	L1 \downarrow	FID \downarrow	FID-VID \downarrow	FVD \downarrow
<i>IMG Effectiveness</i>	Full	0.654	16.93	0.304	2.86E-05	40.19	23.584	225.06
	Finetune	0.596	14.67	0.342	5.35E-05	54.71	31.274	358.31
	t/w IEG	0.615	15.42	0.340	3.85E-05	48.78	29.804	319.96
	End2End-M	0.634	15.84	0.338	3.32E-05	45.05	28.464	285.09
	End2End	0.630	15.74	0.337	3.41E-05	45.23	28.789	289.69
<i>MSM Settings</i>	MSM-4	0.649	16.81	0.308	2.96E-05	40.54	23.704	232.59
	MSM-3	0.644	16.80	0.313	2.98E-05	40.49	24.566	232.47
	MSM-2	0.641	16.68	0.317	3.02E-05	42.58	24.935	236.10
	w/o MSM	0.637	16.50	0.321	3.14E-05	41.26	25.507	256.01
<i>PCS Settings</i>	PCS-0.5	0.654	16.88	0.311	2.95E-05	40.56	24.603	228.19
	PCS-0.4	0.650	16.89	0.312	2.99E-05	41.73	23.708	234.56
	PCS-0.2	0.652	16.72	0.311	2.96E-05	40.99	24.072	226.89
	PCS-0.1	0.654	16.94	0.309	2.95E-05	40.47	23.592	227.32
	w/o PCS	0.632	16.23	0.329	3.07E-05	43.79	25.146	252.33
λ Settings	λ -0.05	0.637	16.59	0.322	3.01E-05	41.76	23.243	233.34
	λ -0.10	0.653	16.80	0.309	2.99E-05	42.04	23.691	234.35
	λ -0.15	0.649	16.77	0.308	2.89E-05	42.62	24.093	234.44
	λ -0.20	0.654	16.93	0.304	2.86E-05	40.19	23.584	225.06
	λ -0.25	0.653	16.71	0.316	2.98E-05	40.47	23.156	230.18



Figure 5: Qualitative comparison against different variants. Red boxes highlight cases of identity switch, while yellow boxes indicate instances of feature contamination.

Effectiveness of Pre-Classified Sampling. By comparing PCS under different sampling ratios, we find that a ratio of 0.3 achieves an optimal trade-off between hard sample abundance and diversity. This setting yields the best performance and effectively alleviates the long-tail data problem.

Hyper-Parameters Analysis on the λ . We conduct a sensitivity analysis on the hyper-parameter λ introduced in Equation (8). Setting λ to 0.20 achieves the best overall performance. This value offers an optimal trade-off between the diffusion reconstruction loss and the identity matching loss. Higher values cause the IC accuracy to plateau while slightly degrading the visual quality.

Effectiveness of MQA. We conduct an experiment in the Appendix to compare MQA with other similarity-based affinity calculation methods.

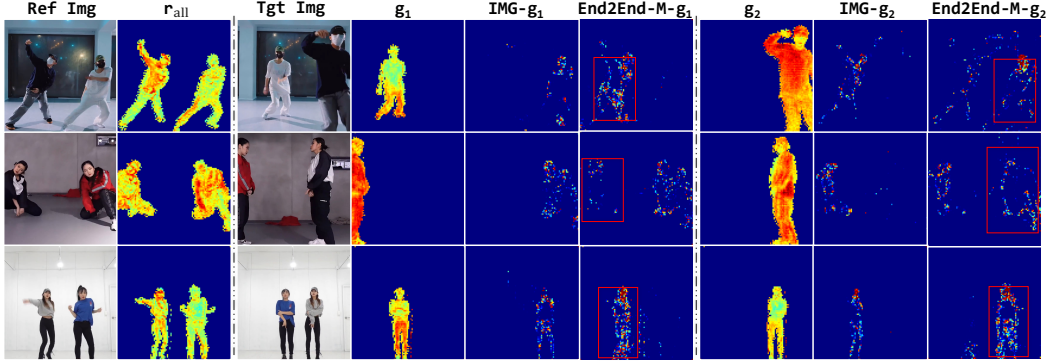


Figure 6: Ideally, the attention distribution should be primarily concentrated on the corresponding reference character located on the opposite side of g_j .

Table 3: Quantitative comparison on frame and video quality metrics. For more details about settings of this benchmark, please refer to [50].

Method	Frame Quality				Video Quality		
	SSIM \uparrow	PSNR \uparrow	LPIPS \downarrow	L1 \downarrow	FID \downarrow	FID-VID \downarrow	FVD \downarrow
DisCo [8]	0.793	29.65	0.239	7.64E-05	77.61	104.57	1367.47
MagicAnime [10]	0.819	29.01	0.183	6.28E-05	40.02	19.42	223.82
MagicPose [12]	0.806	31.81	0.217	4.41E-05	31.06	30.95	312.65
AnimateAnyone [9]	0.795	31.44	0.213	5.02E-05	33.04	22.98	272.98
Follow-Your-Pose-V2 [50]	0.830	31.86	0.173	4.01E-05	26.95	14.56	142.76
EverybodyDance (Ours)	0.879	32.49	0.151	0.92E-05	26.01	12.68	127.36

4.4 Generalizability

On Public Multi-character Benchmark. To validate the generalizability of our method, we also conducted comparisons with the publicly available benchmark provided by Follow-Your-Pose-V2 [50]. This benchmark is distinguished by frequent inter-person occlusions. As shown in Table 3, our method outperforms Follow-Your-Pose-V2 and other SOTA methods across all quality metrics. It should be noted that these metrics primarily reflect overall video fidelity. Since our method lacks explicit occlusion modeling, the foreground-background order during occlusions will be determined randomly.

In Diverse Scenarios. We conducted a comprehensive quantitative evaluation to assess our method’s capabilities in diverse scenarios. Specifically, we benchmarked its performance on challenging multi-character videos containing 3 to 5 individuals, and on the widely-used single-character TikTok [62] benchmark. As shown in Table 4, our proposed method demonstrates superior performance over all competing methods across all key metrics. For qualitative results, please refer to the Appendix.

Cross-Video Motion Transfer. To assess the generalizability of our method for real-world applications, we conduct a cross-video motion transfer experiment. In this setting, a source video provides the motion template used to animate a diverse set of reference images. Moreover, we test the model’s flexibility by reassigning character positions. We reorder the color-coded identities in the target IEG. The result, depicted in Figure 7, is a correctly rendered sequence where the characters’ relative positions are swapped, underscoring our model’s capacity for robust and flexible identity control.

5 Conclusion and Limitation

In this work, we introduce Everybody Dance, a framework that addresses the critical challenge of Identity Correspondence (IC) in multi-character animation. The core of our method is the Identity Matching Graph (IMG), which formalizes the ambiguous problem of IC correctness into an explicit, optimizable graph-structural metric. To construct this graph, our Mask-Query Attention (MQA) efficiently computes edge weights. This graph-based loss works in synergy with our Identity-Embedded Guidance (IEG) together, they form a cohesive guidance-supervision architecture. Finally,

Table 4: Quantitative comparison on multi-character and single-character benchmarks. We group metrics into Frame Quality and Video Quality. Best results are in **bold**.

Scene	Method	Frame Quality				Video Quality	
		SSIM \uparrow	PSNR* \uparrow	LPIPS \downarrow	FID \downarrow	FID-VID \downarrow	FVD \downarrow
<i>More Character</i>	AnimateAnyone [9]	0.606	14.70	0.370	56.66	35.356	401.51
	AnimateAnyone* [9]	0.607	14.92	0.363	64.34	36.308	406.08
	UniAnimate [13]	0.640	15.62	0.338	57.75	29.030	348.91
	Ours	0.671	16.68	0.315	42.84	23.571	261.01
<i>Single Character</i>	AnimateAnyone [9]	0.768	17.85	0.280	52.15	25.864	209.14
	AnimateAnyone* [9]	0.764	17.19	0.291	62.52	25.943	213.68
	End2End	0.770	17.65	0.288	45.25	22.515	186.34
	Ours	0.772	17.78	0.279	40.56	20.294	163.85

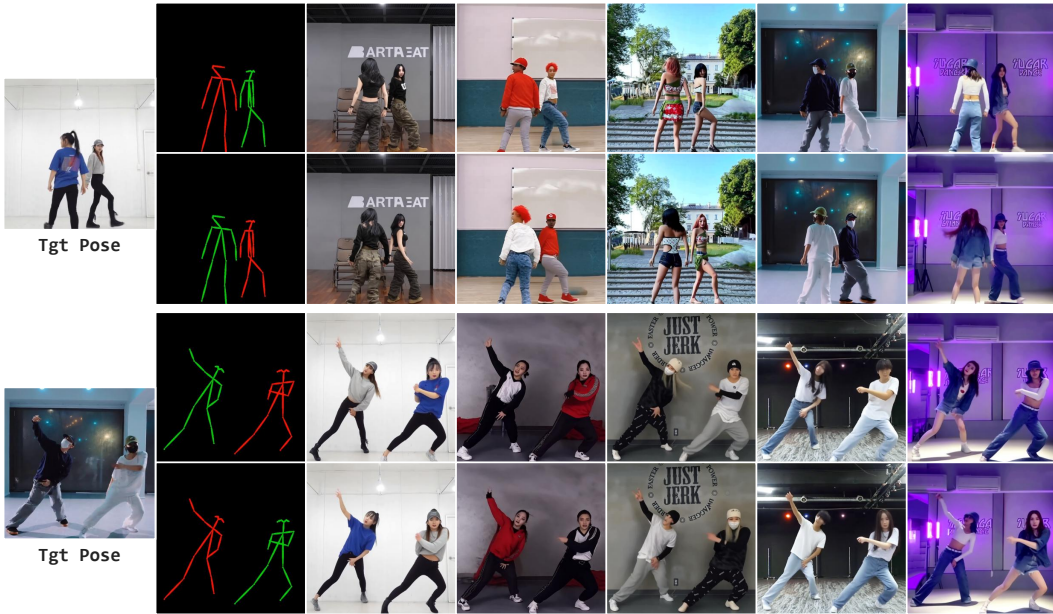


Figure 7: We employ a multi-person video clip as the source pose and use various references to generate animations. We also swap the relative positions of characters in the target pose.

we enhance IC robustness through two targeted strategies: Multi-Scale Matching (MSM) enforces correctness across multiple feature hierarchies, while Pre-Classified Sampling (PCS) addresses challenging, rare training samples. These contributions enable our model to significantly improve identity consistency and visual quality in complex multi-character scenes.

However, our current method is unable to effectively handle scenarios with severe inter-character occlusion. Incorporating 3D datasets [63; 64; 65] presents a promising direction for future work to address this. Furthermore, the performance of our method depends on the accuracy of the upstream instance segmentation model. Finally, our current quantitative evaluation still relies on proxy metrics that measure overall video fidelity. Designing dedicated metrics that can directly and quantitatively evaluate IC correctness remains a significant open problem.

6 Acknowledgement

The authors appreciate the generous support of Li Auto, which provided the financial backing and essential computational resources that made this research possible. The authors also thank our colleagues at the University of Science and Technology of China, Li Auto, and Communication University of China for their insightful discussions and support throughout this project.

References

- [1] da Silva, A. G., M. V. Mendes Gomes, I. Winkler. Virtual reality and digital human modeling for ergonomic assessment in industrial product development: a patent and literature review. *Applied Sciences*, 12(3):1084, 2022.
- [2] Wohlgenannt, I., A. Simons, S. Stieglitz. Virtual reality. *Business & Information Systems Engineering*, 62:455–461, 2020.
- [3] Loeschcke, S., S. Belongie, S. Benaim. Text-driven stylization of video objects. In *European Conference on Computer Vision*, pages 594–609. Springer, 2022.
- [4] Jiang, Y., S. Yang, T. L. Koh, et al. Text2performer: Text-driven human video generation. In *Proceedings of the IEEE/CVF International Conference on Computer Vision*, pages 22747–22757. 2023.
- [5] Chan, C., S. Ginosar, T. Zhou, et al. Everybody dance now. In *Proceedings of the IEEE/CVF international conference on computer vision*, pages 5933–5942. 2019.
- [6] Siarohin, A., S. Lathuilière, S. Tulyakov, et al. First order motion model for image animation. In H. Wallach, H. Larochelle, A. Beygelzimer, F. d'Alché-Buc, E. Fox, R. Garnett, eds., *Advances in Neural Information Processing Systems*, vol. 32. Curran Associates, Inc., 2019.
- [7] Karras, J., A. Holynski, T.-C. Wang, et al. Dreampose: Fashion video synthesis with stable diffusion. In *Proceedings of the IEEE/CVF International Conference on Computer Vision*, pages 22680–22690. 2023.
- [8] Wang, T., L. Li, K. Lin, et al. Disco: Disentangled control for realistic human dance generation. *arXiv preprint arXiv:2307.00040*, 2023.
- [9] Hu, L. Animate anyone: Consistent and controllable image-to-video synthesis for character animation. In *Proceedings of the IEEE/CVF Conference on Computer Vision and Pattern Recognition*, pages 8153–8163. 2024.
- [10] Xu, Z., J. Zhang, J. H. Liew, et al. Magicanimate: Temporally consistent human image animation using diffusion model. In *Proceedings of the IEEE/CVF Conference on Computer Vision and Pattern Recognition*, pages 1481–1490. 2024.
- [11] Zhu, S., J. L. Chen, Z. Dai, et al. Champ: Controllable and consistent human image animation with 3d parametric guidance. In *European Conference on Computer Vision (ECCV)*. 2024.
- [12] Chang, D., Y. Shi, Q. Gao, et al. Magicpose: Realistic human poses and facial expressions retargeting with identity-aware diffusion. In *Forty-first International Conference on Machine Learning*. 2023.
- [13] Wang, X., S. Zhang, C. Gao, et al. Unianimate: Taming unified video diffusion models for consistent human image animation. *ArXiv*, abs/2406.01188, 2024.
- [14] Zhang, Y., J. Gu, L.-W. Wang, et al. Mimicmotion: High-quality human motion video generation with confidence-aware pose guidance. *arXiv preprint arXiv:2406.19680*, 2024.
- [15] Ho, J., A. Jain, P. Abbeel. Denoising diffusion probabilistic models. *Advances in neural information processing systems*, 33:6840–6851, 2020.
- [16] Sohl-Dickstein, J., E. Weiss, N. Maheswaranathan, et al. Deep unsupervised learning using nonequilibrium thermodynamics. In *International conference on machine learning*, pages 2256–2265. PMLR, 2015.
- [17] Luo, C., D. Di, X. Yang, et al. Trame: Trajectory-anchored multi-view editing for text-guided 3d gaussian manipulation. *IEEE Transactions on Multimedia*, 2025.
- [18] Di, D., J. Yang, C. Luo, et al. Hyper-3dg: Text-to-3d gaussian generation via hypergraph. *International Journal of Computer Vision*, 133(5):2886–2909, 2025.

- [19] Song, Y., J. Sohl-Dickstein, D. P. Kingma, et al. Score-based generative modeling through stochastic differential equations. *arXiv preprint arXiv:2011.13456*, 2020.
- [20] Song, J., C. Meng, S. Ermon. Denoising diffusion implicit models. *arXiv preprint arXiv:2010.02502*, 2020.
- [21] Liu, L., Y. Ren, Z. Lin, et al. Pseudo numerical methods for diffusion models on manifolds. In *International Conference on Learning Representations*. 2022.
- [22] Tian, L., Q. Wang, B. Zhang, et al. Emo: Emote portrait alive-generating expressive portrait videos with audio2video diffusion model under weak conditions. *arXiv preprint arXiv:2402.17485*, 2024.
- [23] Lu, C., Y. Zhou, F. Bao, et al. Dpm-solver: A fast ode solver for diffusion probabilistic model sampling in around 10 steps. *Advances in Neural Information Processing Systems*, 35:5775–5787, 2022.
- [24] Heusel, M., H. Ramsauer, T. Unterthiner, et al. Gans trained by a two time-scale update rule converge to a local nash equilibrium. *Advances in neural information processing systems*, 30, 2017.
- [25] Saito, M., E. Matsumoto, S. Saito. Temporal generative adversarial nets with singular value clipping. In *ICCV*. 2017.
- [26] Xie, Q., Y. Ma, D. Di, et al. Moca: Identity-preserving text-to-video generation via mixture of cross attention. In *ACM Multimedia Asia*. 2025.
- [27] Wu, J. Z., Y. Ge, X. Wang, et al. Tune-a-video: One-shot tuning of image diffusion models for text-to-video generation. *2023 IEEE/CVF International Conference on Computer Vision (ICCV)*, pages 7589–7599, 2022.
- [28] Zhou, D., W. Wang, H. Yan, et al. Magicvideo: Efficient video generation with latent diffusion models. *ArXiv*, abs/2211.11018, 2022.
- [29] Lu, H., G. Yang, N. Fei, et al. Vdt: General-purpose video diffusion transformers via mask modeling. In *International Conference on Learning Representations*. 2023.
- [30] Gao, Y., J. Huang, X. Sun, et al. Matten: Video generation with mamba-attention. *ArXiv*, abs/2405.03025, 2024.
- [31] Li, K., X. Li, Y. Wang, et al. Videomamba: State space model for efficient video understanding. In *European Conference on Computer Vision*. 2024.
- [32] Lu, Y., Y. Liang, L. Zhu, et al. Freelong: Training-free long video generation with spectralblend temporal attention. *ArXiv*, abs/2407.19918, 2024.
- [33] Zhou, S., P. Yang, J. Wang, et al. Upscale-a-video: Temporal-consistent diffusion model for real-world video super-resolution. *2024 IEEE/CVF Conference on Computer Vision and Pattern Recognition (CVPR)*, pages 2535–2545, 2023.
- [34] Siarohin, A., O. Woodford, J. Ren, et al. Motion representations for articulated animation. In *CVPR*. 2021.
- [35] Li, Y., C. Huang, C. C. Loy. Dense intrinsic appearance flow for human pose transfer. In *Proceedings of the IEEE/CVF conference on computer vision and pattern recognition*, pages 3693–3702. 2019.
- [36] Kissel, C., C. Kümmel, D. Ritter, et al. Pose-guided sign language video gan with dynamic lambda. *arXiv preprint arXiv:2105.02742*, 2021.
- [37] Zablotskaia, P., A. Siarohin, B. Zhao, et al. Dwnet: Dense warp-based network for pose-guided human video generation. *arXiv preprint arXiv:1910.09139*, 2019.

- [38] Yoon, J. S., L. Liu, V. Golyanik, et al. Pose-guided human animation from a single image in the wild. In *Proceedings of the IEEE/CVF Conference on Computer Vision and Pattern Recognition*, pages 15039–15048. 2021.
- [39] Fu, J., S. Li, Y. Jiang, et al. Stylegan-human: A data-centric odyssey of human generation. In *European Conference on Computer Vision*. 2022.
- [40] Jiang, S., H. Jiang, Z. Wang, et al. Humangen: Generating human radiance fields with explicit priors. *2023 IEEE/CVF Conference on Computer Vision and Pattern Recognition (CVPR)*, pages 12543–12554, 2022.
- [41] Zhang, P., L. Yang, J. Lai, et al. Exploring dual-task correlation for pose guided person image generation. *2022 IEEE/CVF Conference on Computer Vision and Pattern Recognition (CVPR)*, pages 7703–7712, 2022.
- [42] Sarkar, K., D. Mehta, W. Xu, et al. Neural re-rendering of humans from a single image. In *European Conference on Computer Vision*. 2021.
- [43] Albahar, B., S. Saito, H.-Y. Tseng, et al. Single-image 3d human digitization with shape-guided diffusion. *SIGGRAPH Asia 2023 Conference Papers*, 2023.
- [44] Shao, R., Y. Pang, Z. Zheng, et al. Human4dit: 360-degree human video generation with 4d diffusion transformer. *arXiv preprint arXiv:2405.17405*, 2024.
- [45] Yuan, S., J. Huang, X. He, et al. Identity-preserving text-to-video generation by frequency decomposition. In *Proceedings of the Computer Vision and Pattern Recognition Conference*, pages 12978–12988. 2025.
- [46] Yin, X., D. Di, L. Fan, et al. Grpose: Learning graph relations for human image generation with pose priors. In *Proceedings of the AAAI Conference on Artificial Intelligence*, vol. 39, pages 9526–9534. 2025.
- [47] Rombach, R., A. Blattmann, D. Lorenz, et al. High-resolution image synthesis with latent diffusion models. In *Proceedings of the IEEE/CVF Conference on Computer Vision and Pattern Recognition*, pages 10684–10695. 2022.
- [48] Zhang, L., A. Rao, M. Agrawala. Adding conditional control to text-to-image diffusion models. In *Proceedings of the IEEE/CVF international conference on computer vision*, pages 3836–3847. 2023.
- [49] Fei, Z., D. Li, D. Qiu, et al. Ingredients: Blending custom photos with video diffusion transformers, 2025.
- [50] Xue, J., H. Wang, Q. Tian, et al. Towards multiple character image animation through enhancing implicit decoupling. In *The Thirteenth International Conference on Learning Representations*. 2025.
- [51] Ronneberger, O., P. Fischer, T. Brox. U-net: Convolutional networks for biomedical image segmentation. In *Medical image computing and computer-assisted intervention–MICCAI 2015: 18th international conference, Munich, Germany, October 5-9, 2015, proceedings, part III 18*, pages 234–241. Springer, 2015.
- [52] Ravi, N., V. Gabeur, Y.-T. Hu, et al. Sam 2: Segment anything in images and videos. *arXiv preprint arXiv:2408.00714*, 2024.
- [53] Vaswani, A. Attention is all you need. *Advances in Neural Information Processing Systems*, 2017.
- [54] Yang, Z., A. Zeng, C. Yuan, et al. Effective whole-body pose estimation with two-stages distillation. *2023 IEEE/CVF International Conference on Computer Vision Workshops (ICCVW)*, pages 4212–4222, 2023.
- [55] Fang, H.-S., J. Li, H. Tang, et al. Alphapose: Whole-body regional multi-person pose estimation and tracking in real-time. *IEEE Transactions on Pattern Analysis and Machine Intelligence*, 2022.

- [56] Loper, M., N. Mahmood, J. Romero, et al. Smpl: A skinned multi-person linear model. In *Seminal Graphics Papers: Pushing the Boundaries, Volume 2*, pages 851–866. 2023.
- [57] Isola, P., J.-Y. Zhu, T. Zhou, et al. Image-to-image translation with conditional adversarial networks. In *Proceedings of the IEEE conference on computer vision and pattern recognition*, pages 1125–1134. 2017.
- [58] Netravali, A. N. *Digital pictures: representation, compression, and standards*. Springer, 2013.
- [59] Wang, Z., A. C. Bovik, H. R. Sheikh, et al. Image quality assessment: from error visibility to structural similarity. *IEEE transactions on image processing*, 13(4):600–612, 2004.
- [60] Zhang, R., P. Isola, A. A. Efros, et al. The unreasonable effectiveness of deep features as a perceptual metric. In *Proceedings of the IEEE conference on computer vision and pattern recognition*, pages 586–595. 2018.
- [61] Unterthiner, T., S. van Steenkiste, K. Kurach, et al. Fvd: A new metric for video generation. 2019.
- [62] Jafarian, Y., H. S. Park. Learning high fidelity depths of dressed humans by watching social media dance videos. In *Proceedings of the IEEE/CVF Conference on Computer Vision and Pattern Recognition*, pages 12753–12762. 2021.
- [63] Ng, E., D. Xiang, H. Joo, et al. You2me: Inferring body pose in egocentric video via first and second person interactions. *CVPR*, 2020.
- [64] Liang, H., W. Zhang, W. Li, et al. Intergen: Diffusion-based multi-human motion generation under complex interactions. *International Journal of Computer Vision*, 132(9):3463–3483, 2024.
- [65] Siyao, L., T. Gu, Z. Yang, et al. Duolando: Follower gpt with off-policy reinforcement learning for dance accompaniment. In *The Twelfth International Conference on Learning Representations*.